Rincón, A.; Moreno, R.; Chinelatto, ASA.; Gutierrez-Gonzalez, CF.; Rayón Encinas, E.; Salvador Moya, MD.; Borrell Tomás, MA. (2014). Al2O3-3YTZP-Graphene multilayers produced by tape casting and spark plasma sintering. Journal of the European Ceramic Society. 34(10):2427-2434. doi:10.1016/j.jeurceramsoc.2014.02.011.

Al_2O_3-3YTZP-Graphene multilayers produced by tape casting and spark plasma sintering

Acacio Rincón[1], Rodrigo Moreno[1], Adriana S. A. Chinelatto[2], Carlos F. Gutierrez[3], Emilio Rayón[4], María Dolores Salvador[4], Amparo Borrell[4]*

[1]Instituto de Cerámica y Vidrio (ICV), Consejo Superior de Investigaciones Científicas (CSIC), E-28049 Madrid, Spain

[2]Universidade Estadual de Ponta Grossa, Av. Carlos Cavalcanti, 4748 - Uvaranas, Ponta Grossa - PR, 84030-900 Brasil

[3]Centro de Investigación en Nanomateriales y Nanotecnología (Consejo Superior de Investigaciones Científicas, Universidad de Oviedo, Principado de Asturias), Parque Tecnológico de Asturias, 33428 Llanera, Spain

[4]Instituto de Tecnología de Materiales (ITM), Universitat Politècnica de València (UPV), Camino de Vera s/n, 46022 Valencia, Spain

*Corresponding autor: Instituto de Tecnología de Materiales (ITM), Universitat Politècnica de València (UPV), Camino de Vera s/n, 46022 Valencia, Spain. E-mail: aborrell@upv.es (A. Borrell)

ABSTRACT

This work aims to establish a colloidal route to obtain laminates of alumina-zirconia combining layers with and without graphene. Green tapes of alumina, alumina with 5vol.% of 3Y-TZP and alumina with 5vol.% of 3Y-TZP and graphene-oxide (2vol.%) were obtained by aqueous tape casting. It is

possible to design materials for different structural applications with a controlled microstructure with a high number of different layers. The tapes were punched into 20-mm discs, joined to form laminates alternating up to 18-layers, and sintered in one-step by spark plasma sintering (SPS) at 1400 ºC. It has demonstrated that there is a significant graphite diffusion provoked by the required graphite holders into the SPS-furnace. Dense laminates with layer thicknesses ~100 μm and good cohesion between layers were obtained. Nanoindentation results showed that hardness and elastic modulus values were higher than 27 GPa and 300 GPa, respectively, and similar for all layers.

Keywords: Multilayers; Mechanical properties; Tape casting; Spark plasma sintering, Graphene

1. Introduction

The incorporation of carbon derivatives, such as carbon nanotubes (CNTs), carbon nanofibers (CNFs), diamond nanoparticles and graphene as secondary phases in composites, is receiving increasing attention due to their unique combination of properties that enhance when they are added in small concentrations.[1-5] CNTs and CNFs have been largely used as suitable reinforcing agents of different materials for many applications such as prostheses fabrication, lithium ion batteries, proton exchange membranes, etc.[6-9] Single-wall carbon nanotubes (SWCNTs) have been successfully used for these purposes, although the difficult homogenisation within the matrix has still important limitations.[10,11] Consequently, the studies regarding the use of multi-wall carbon nanotubes (MWCNTs), which are much easier to disperse in a

matrix (especially in water), have received greater attention. The most widely studied ceramic matrices are oxides such as alumina, zirconia, mullite, etc.,[12-16] and also non-oxidic ceramics such as silicon nitride in which new properties are achieved, for example electrical conductivity, as well as mechanical reinforcement.[17-19] The use of diamond nanoparticles has huge interest for improving the contact-mechanical and tribological properties of the composites.[20,21]

Graphene is considered one of the most singular materials for reinforcing polymers, metals and ceramics. Among the wide number of applications of graphene those referring to ceramics have not yet achieved the expected consideration, but it has been already demonstrated its beneficial effect in the enhancement of conductivity and reinforced mechanical properties, to mention only a couple.[22-26] In spite of these clear advantages, there are two main topics that are far to be already solved: the synthesis of the graphene sheets, on one hand, and the preparation of homogeneous mixtures of graphene in a ceramic powder matrix, on the other hand. Graphene is usually obtained from graphite flakes by liquid exfoliation, milling or sonication and by the so-called Hummers' method,[27] in which the oxidation of graphite to graphitic oxide is accomplished by treating graphite with essentially a water-free mixture of concentrated sulphuric acid, sodium nitrate and potassium permanganate. Graphene is obtained by reduction of this graphitic oxide for which hydrazine is often used. Moreover, the use of a hydrophilic form of graphite (as an oxide) has important advantages from the point of view of processing and dispersibility, as it allows an easy mixing in aqueous suspensions if colloidal interactions are adequately controlled.[28,29]

The polar character of graphene oxide (GO) allows the dispersion by electrostatic or electrosteric forces facilitating its dispersion in polar solvents such as water. Since the properties of GO are worse than those of the reduced graphene, materials obtained with GO must be reduced in a further step, normally by using sintering cycles under reducing atmosphere.[30]

As stated earlier, the most studied ceramic matrices for such GO-reinforced ceramics have been alumina and Y-TZP, as it was expected that the carbon nanodispersoids could provide the required strengthening. It is well known that small zirconia additions can enhance the mechanical behaviour of an alumina matrix by transformation toughening.[31,32]

From a structural point of view, the major concern is to increase the mechanical performance by either the action of reinforcing mechanisms or by reducing the flaws effect with tailored microstructures, which make the material to become flaw tolerant. In this sense, laminates have demonstrated their suitability for obtaining materials with superior properties to those of the individual components.[33-36] Laminates can improve mechanical performance using either laminates with a weak interface that deflects cracks, thus preventing catastrophic failure or laminates with strong interfaces designed on the basis of residual stress development in the layers during cooling from the sintering temperature. Furthermore, from an electrical features point of view, to achieve the configuration of a series of electrical and non electrical conductive layered material it should be very interesting to develop microelectronic devices with high performances.

The most widely studied laminate system is that formed by alumina-zirconia, in which a broad interval of thermal strains can be reached by modulating the thermal expansion coefficient of the constituent layers and/or the extent of zirconia phase transformation. The manufacture of these laminates needs the use of techniques allowing a simple processing and lamination process. For such purpose colloidal shaping techniques have been extensively used, especially simple processes such as sequential slip casting and tape casting.[37-40]

In contrast with the extensive bibliography about alumina-zirconia laminates and the increasing effort on the use of carbon nanodispersoids on single phase materials, the effect of graphene additions on the processing, on mechanical performance and electrical conductivity of alumina-zirconia composites is very scarce.[41]

In this context the objective of this work was to study the processing of alumina-zirconia laminates comprising layers with and without graphene, obtained by spark plasma sintering, in order to evaluate the effect of the graphene addition on the properties of alumina-zirconia composite layers. Furthermore, by means of staking layers with and without graphene, it has been achieved the construction of a ceramic compound formed by electrical layers isolated by non electrical layers. In a previous paper, the preparation of the individual layers constituting the laminate was studied in terms of suspensions stabilisation, rheological behaviour and tape casting performance.[42] This paper focuses on the lamination of those tapes into specific microarchitectures combining layers of alumina-zirconia with and without graphene.

2. Experimental procedure

Two commercial ceramic powders were used as starting materials: an α-alumina powder (Ceralox, Condea HPA05, USA) with an average particle size of 0.35 μm and a specific surface area of 9.5 $m^2 \cdot g^{-1}$, and a nanosized zirconia doped with 3 mol.% of Y_2O_3 (TZ3YE, Tosoh, Japan) with an average particle size of 100 nm and a specific surface area of 14.5 $m^2 \cdot g^{-1}$. A monolayer graphene oxide (Nanoinnova Technologies, Spain), simply referred to as GO, with average lengths and thicknesses in the range of 1 to 4 μm and 0.7 to 1.2 nm, respectively, and a surface area of ~103 $m^2 \cdot g^{-1}$ was also used as a secondary reinforcing phase.

Multilayer materials were prepared by simple lamination (under atmospheric conditions and hand pressure gluing with a few water drops) of dry layers obtained by aqueous tape casting of concentrated alumina suspension containing zirconia as secondary phase (referred to as AZ), and layers of AZ containing 2 vol.% (0.5 wt.%) with regard to dry ceramic powders of graphene oxide as a dispersed phase (referred to as AZGO). Alumina (A) layers were also prepared to allow comparison with AZ ones. Since alumina is very well known no further rheological studies were done, so that the tapes were prepared as described in previous work.[42] The relative volume ratio of alumina to zirconia was 95:5 vol.% (92.5:7.5 wt.%). The suspensions were prepared to solids loadings of 53 vol.% for A and AZ, and 40 vol.% for AZGO by sonication in pulsed mode (0.5 cycles). The details of the rheological studies and the optimisation of tape casting performance were reported in a previous work.[42] Tape casting suspensions were prepared with an acrylic latex emulsion with a content of active matter of 55 wt.% (Duramax B-1000, Rohm &

Haas, PA, USA), which was used as a binder adding 15 wt.% (weight of as-supplied product related to the total solid content, i.e. by 8.3 wt.% of active matter), and a defoamer (KS 1115, Zschimmer & Schwarz, Germany) to allow the elimination of air bubbles originated during homogenisation, which was added in a concentration of 0.15 wt.%. The so-prepared mixtures were kept under mechanical stirring for 20 min to achieve homogenisation before casting. Tape casting was conducted onto a Mylar film using a single blade geometry casting head; the blade height was set at 200 μm with a casting speed of 50 $mm \cdot s^{-1}$.

Three families of laminates were produced for this study: 1) alternating layers of A and AZ, the laminate being referred to as A/AZ; 2) alternating layers of AZ and AZGO, which was referred to as AZ/AZGO, and 3) alternating the three types of layers, A/AZ/AZGO**.** In Fig. 1 a schematic flow chart of the lamination process is shown. Tapes were first cut into discs with 2 cm in diameter, and the discs were then laminated applying a small pressure and using a few drops of water as gluing agent. Symmetric laminates with 9-layers were obtained.

To obtain the sintered materials two stacks of 9 layers each were introduced into a 20-mm-diameter graphite die. The architecture of the different green laminates formed from the tailored stacks can be seen in the picture. The stacks were sintered using a spark plasma sintering (SPS) apparatus HP D25/1 (FCT Systeme GmbH, Rauenstein, Germany) at temperature of 1400 ºC and 80 MPa of pressure to obtain fully sintered bulk materials. The tests were carried out under vacuum at a heating rate of 100 $ºC \cdot min^{-1}$ with a 1 min dwelling time at the maximum temperature.

Sintered samples were fractured on their cross-section and were polished to 0.5 mm using SiC paper and diamond suspension. Resultant layers were observed with optical microscope Nikon LV-100 under dark field illumination. The fracture surface was analysed by using a field emission gun scanning electron microscope (FE-SEM, HITACHI S-4800, SCSIE of the University of Valencia).

Raman spectra were determined on the cross-section of polished samples except for a sample that was analysed after fracture to diminish the possible contamination of the polishing procedure or graphene loss. The measurements were performed at room temperature with a Renishaw inVia spectrometer with λ=514.5 nm laser. A 100x objective was used to locate the 3 μm diameter spot area of analysis on sample. Two spectral ranges were scanned for each layer, 100-800 cm^{-1} and 1000-3200 cm^{-1} with 2 cm^{-1} step resolution. The incident power was carefully programmed to avoid laser induce heating.

Vickers microhardness (HV) was acquired using a Shimadzu HMV tester under a 0.2 Kg indentation load. Hardness (*H*) and modulus (*E*) were analysed by a nanoindenter G-200 of Agilent Technol. (Inc., Santa Clara, CA) under a 1200 nm constant indentation depth program. A Berkovich tip was used after calibration of the function area in fused silica. Stiffness was recorded in depth by Continuous Stiffness Measurement (CSM). The Poisson's coefficient was 0.23 for all calculations considering a fully dense material. In this regard, the wide range of reported Poisson's coefficient for alpha alumina and tetragonal zirconia depends on the porosity and the level of defects in the

microstructure.[43] The resulting reduced modulus has been also reported in this manuscript in order to visualise the influence of this coefficient.

3. Results and discussion

Homogeneous, dense laminates were obtained after heating at 1400 ºC by SPS. Fig. 2 shows the microarchitecture of the three multilayers as observed by optical microscopy. Obviously the external surfaces resulted damaged after the cycle due to the interaction with graphite dies, but the layers configuration remains and the interfaces are sharp and well defined. The picture of Fig. 3 corresponds to a higher magnification image showing a detailed view of the microstructure at the interfaces between A, AZ and AZGO layers. This picture demonstrates the clear, sharp interfaces and the uniformity of the layers.

The microstructure of the fracture surfaces of the different layers (A, AZ, and AZGO) in the A/AZ/AZGO laminate can be observed in Fig. 4. FE-SEM observations of these fracture surfaces show a high degree of densification without apparent macroscopic defects or porosity. As observed in the microphotographs, faceted grains of about 0.25 μm are obtained in any of the layers. These images corroborate that the conditions employed for the SPS procedure were adequate. The presence of some isolated nanosheets within the A/AZ/AZGO layers was captured (indicated by an arrow). These films were observed at higher magnification (Fig. 5) and were revealed as sheets with planar dimensions of several microns but only few nanometres thin. Similar morphological aspect has been reported for few-layered graphene or graphene oxide nanoplatelets.[44] Nevertheless, the identification of graphene flakes is a

major hurdle and scanning electron microscopy technique is not an appropriated tool for this aim.

In order to confirm that graphene remains in the reduced form inside the AZGO layers, Raman spectroscopy analysis was performed for such layers. The α-Al_2O_3 and tetragonal zirconia (3YTZP) have been well characterized by Raman spectroscopy showing bands centred at 378 cm^{-1}, 416 cm^{-1}, 429 cm^{-1}, 576 cm^{-1}, 644 cm^{-1} and 750 cm^{-1} for alumina and 144 cm^{-1}, 268 cm^{-1}, 314 cm^{-1}, 458 cm^{-1} and 650 cm^{-1} for tetragonal zirconia.[45,46] Fig. 6 shows the spectra obtained on the cross-section of A and AZ layers indicating that the unique phases present in these layers are α-Al_2O_3 and 3YTZP+α-Al_2O_3, respectively, as expected.

Nevertheless, graphene bands are centred at the same wavelength than those of graphite. For a 514.5 nm laser these bands are found at 1370 cm^{-1}, also named D-band that is characteristic of disorder, at 1583 cm^{-1} or G-band that is assigned to a graphitic structure and it is good indicator of graphene layers; and the 2700 cm^{-1} band or 2D band that can be also used to determine the number of graphene layers. It has been shown [46] that as the number of layers increases, the G-band position shifts to lower frequencies. Fig. 7 screens the spectra obtained in the spectral range of Raman wavelengths in which graphene must be detected. These results reveal the presence of the characteristic G, D and 2D bands on all analyzed layers and samples, even inside the layers that did not contain any carbon source (A and AZ layers). This fact demonstrates that there is a significant graphite diffusion provoked by the required graphite holders into the SPS furnace. This hypothesis was corroborated when the same spectra was acquired on the grey coloured

samples' surfaces instead of their cross-sections. The diffusion mechanism of graphite inside the ceramic material in SPS is not yet well understood. Consequently, it was not possible to distinguish the graphene signal by Raman analysis because the graphite signal or by the carbon formed from the decomposition of the polymer masks the possible graphene response. Furthermore, Centeno et al. [25] showed that graphene basal plane is preferentially oriented perpendicularly to the direction of the pressure applied during SPS. Consequently, the surface of graphene exposed to the Raman's source is very small when samples are analyzed on their cross-section. However mechanical properties seem to be affected by the addition of graphene while graphite contamination does not negatively affect, as shown below.

Mechanical properties of single layers were determined by microhardness measurements and by nanoindentation technique. Fig. 8 shows several arrays of Berkovich imprints performed at a constant 1200 nm depth by nanoindentation technique. The microstructure shows that A and AZ layers have densified to suitable values, whereas the layers containing GO have considerably higher porosity. The different layers were obtained at similar tape casting speed and blades height, but there is a clear difference, the A layer being the thickest while the AZGO one is the thinnest. There is an inverse relation between viscosity of the slurry and final thickness. The viscosities of the A, AZ and AZGO tape casting suspensions were 819, 480 and 523 mPa·s (at a shear rate of 250 s^{-1}, which was roughly calculated to be the shear rate when the slurry is passing through the blade). The corresponding average thicknesses are 75, 60, and 50 μm, respectively.

Fig. 9 shows the resulting *H* and *E* curves as a function of the indentation depth obtained by nanoindentation technique. Vickers hardness was also acquired for each layer and these results are summarised in Table 1.

It must be remarked that the laminated material displays high nanomechanical properties that can be explained by the high densification and small grain size achieved by tapes lamination and further non-conventional sintering by SPS technique. The content of either ZrO_2 or graphene slightly diminishes the hardness and modulus with regard to that of the pure α-alumina and these results are in good agreement with those reported for fully dense materials.[47-50] The nanomechanical properties were also investigated along all the width of the laminate in order to detect possible gradients in densification. Fig. 10 shows the elastic modulus (Fig. 10a) and the nanohardness (Fig. 10b) profiles for indentations performed at 300 nm maximum depth (Fig. 10c). These curves demonstrate that the density along the cross-section of sample is constant and the mechanical properties remain constant inside the entire sample, without any differences at the various layers comprising the laminate. The dispersion of values for a single layer is explained because at low penetration depths the response of single phases is distinguished. 3Y-TZP is found in the form of small aggregates in the alumina layer (inset figure). Consequently, the variability of results indicates the presence of some aggregates of 3Y-TZP grain or dense alumina beyond the indenter. This tendency to form nanoaggregates is, unfortunately, very usual in the preparation of AZ composites, in spite of the enhancement of the dispersion using colloidal processing.

In this work, the electrical conductivity of the A, AZ and AZGO layers were confirmed by a very simple method. Using a two probe electrical multimeter device, it was confirmed that the electrical resistance was below 10 Ohm on the AZGO layers while open circuit (Megaohm) was registered on the surface on the A and AZ layers. In order to ensure a good electrical contact very thin gold wire probes were used. In an incoming paper, the electrical conductivity performance of these laminates will be further studied using more adequate techniques.

In summary the results shown in this paper demonstrate that it is possible to tailor ceramic laminates comprising any number of layers comprising graphene or not, as desired. While the mechanical properties at every layer are not so different, the electrical conductivity is only found in layers with graphene.

4. CONCLUSIONS

This paper reports for the first time the preparation of Al_2O_3-3YTZP-graphene multilayer materials combining tape casting and fast spark plasma sintering technique with good cohesion and high mechanical properties.

Raman spectroscopy has been used to study in detail the layers and to evaluate and optimize the in situ graphene thermal reduction process in the SPS. During the composite fabrication process, the material sintering and the GO thermal reduction occurs simultaneously, and also, we have demonstrate that there is a significant graphite diffusion provoked by the required graphite holders into the SPS furnace. Therefore, it was not possible to distinguish the graphene signal by Raman analysis because the graphite signal masks the possible graphene response.

From these results it can be concluded that it is possible to design materials with a controlled microstructure with a high number of different layers comprising graphene or not, as desired. The nanomechanical properties at the different layers of the laminate are rather similar, so that the presence of graphene is not deleterious for the laminate integrity and the layers properties. This could be very advantageous for the macroscopic mechanical behavior of the laminate, in which the presence of the interfaces could contribute to enhance the laminate behavior. This would require the evaluation of bending strength, which is out of the scope of the present investigation.

Acknowledgements

This work has been supported by Spanish Ministry of Economy and Competitiviness (MAT2012-31090). A. S. A. Chinelatto thanks to CAPES - Programa Ciências sem Fronteiras (Brazil) for the concession of a fellowship for post-doctoral sabbatical grant in ICV-CSIC, Spain. A. Borrell, acknowledges the Spanish Ministry of Science and Innovation for her Juan de la Cierva contract (JCI-2011-10498) and the Generalitat Valenciana by the financial support for the BEST/2012/302 grant. Authors thank to Nanoinnova Technologies (Spain) for supplying the graphene oxide and helpful discussions.

REFERENCES

[1] Kim YA, Hayashi T, Endo M, Dresselhaus MS. Carbon nanofibers, Ch 3 in Springer Handbook of Nanomaterials, Bhushan B, ed. Springer-Verlag Berlin Heidelberg 2007.

[2] Monthioux M, Serp P, Flahaut E, Razafinimanana M, Laurent C, Peigney A. Introduction to carbon nanotubes, Ch. 7 in Springer Handbook of Nanotechnology, Bhushan B, ed. Springer-Verlag Berlin Heidelberg 2011.

[3] Thostenson ET, Rhen ZF, Chou TW. Advances in the science and technology of carbon nanotubes and their composites: a review. Composites Sci Tech 2001;61:1899-912.

[4] Curtin WA, Sheldon BW. CNT-reinforced ceramics and metals. Mater Today 2004;7:44-9.

[5] Zapata-Solvas E, Gómez-García D, Domínguez-Rodríguez A. Towards physical properties tailoring of carbon nanotubes-reinforced ceramic matrix composites. J Eur Ceram Soc 2012;32(12):3001-20.

[6] Ahammad AJS, Lee JJ, Rahman MA. Electrochemical sensors based on carbon nanotubes. Sensors 2009;9:2289-319.

[7] Fu K, Yildiz O, Bhanushali H, Wang Y, Stano K, Xue L, Zhang X, Bradford PD. Aligned carbon nanotube-silicon sheets: a novel nano-architecture for flexible lithium ion battery electrodes. Adv Mater 2013;25:5109-14.

[8] Borrell A, Torrecillas R, Rocha VG, Fernández A. Alumina-carbon nanofibers nanocomposites obtained by spark plasma sintering for proton exchange membrane. Fuel Cells 2012;4:599-605.

[9] Dusza J, Blugan G, Morgiel J, Kuebler J, Inam F, Peijs T, Reece MJ, Puchya V. Hot pressed and spark plasma sintered zirconia/carbon nanofiber composites. J Eur Ceram Soc 2009;29:3177-84.

[10] Zhan GD, Kuntz JD, Wan J, Mukherjee AK. Single-wall carbon nanotubes as attractive toughening agents in alumina based nanocomposites. Nat Mater 2003;61:1899-1912.

[11] Wei T, Fan Z, Luo G, Wei F, Zhao D, Fan J. The effect of carbon nanotubes microstructures on reinforcing properties of SWNTs/alumina composite. Mater Res Bull 2008;43:2806-9.

[12] Balani K, Zhang T, Karakoti A, Li WZ, Seal S, Agarwal A. In situ carbon nanotube reinforcements in plasma sprayed aluminium oxide nanocomposite coating. Acta Mater 2008;56:571-9.

[13] Garmendia N, Santacruz I, Moreno R, Obieta I. Zirconia-MWCNT nanocomposites for biomedical applications obtained by colloidal processing. J Mater Sci: Mater Med 2010;21:1445-51.

[14] Fan J, Zhao D, Wu M, Xu Z, Song J. Preparation and microstructure of multi-wall carbon nanotubes toughened Al_2O_3 composite. J Am Ceram Soc. 2006;89:750-3.

[15] Borrell A, Rocha VG, Torrecillas R, Fernández A. Surface coating on carbon nanofibers with alumina precursor by different synthesis routes. Comp Sci Technol 2011;71(1):18-22.

[16] Rodríguez D, Cano IG, Fernández J, Fariñas JC, Moreno R. Rheological behaviour of submicron mullite-carbon nanofiber suspensions for atmospheric Plasma Spraying coatings. J Eur Ceram Soc 2014;34:475-83.

[17] Balázsi C, Shen Z, Kónya Zs, Kasztovszky F, Wéber Z, Vértesy LP, Biró I, Kiricsi P, Arató P. Processing of carbon nanotube reinforced silicon nitride composites by spark plasma sintering. Comp Sci Technol 2005;65(5):727-33.

[18] Pasupuleti S, Peddetti R, Santhanam S, Jena KP, Wing ZN, Hecht M, Halloran JP. Toughening behavior in a carbon nanotube reinforced silicon nitride composite. Mater Sci Eng A 2008;491(1-2):224-9.

[19] Belmonte M, González-Julián J, Miranzo P, Osendi MI. Spark plasma sintering: A powerful tool to develop new silicon nitride-based materials, J Eur Ceram Soc 2010;30:2937-46.

[20] Ownby PD, Liu J. Normal-pressure hot-pressing of α-alumina-diamond composites. J Am Ceram Soc1991;74:2666-8.

[21] Huang S, Swarnakar AK, Vanmeensel K, Vleugels J. Diamond dispersed Si_3N_4 composites obtained by pulsed electric current sintering. J Eur Ceram Soc 2013;33:1237-47.

[22] Singh V, Joung D, Das S, Khondaker SI, Seal S. Graphene based materials: past, present and future. Progress Mater Sci 2011;56:1178-1271.

[23] Dusza J, Morgiel J, Duszová A, Kvetková L, Nosko M, Kun P, Balázsi C. Microstructure and fracture toughness of Si_3N_4+graphene platelet composites. J Eur Ceram Soc 2012;32(12):3389-97.

[24] Porwal H, Tatarko P, Grasso S, Reece MJ. Graphene reinforced alumina nano-composites. Carbon 2013;64:359-69.

[25] Centeno A, Rocha VG, Alonso B, Fernández A, Gutiérrez-González CF, Torrecillas R., Zurutuza A, Graphene for tough and electroconductive alumina ceramics. J Eur Ceram Soc 2013;33:3201-10.

[26] Miranzo P, Ramírez C, Román-Manso B, Garzón L, Gutierrez HR, Terrones M, Ocal C, Osendi MI. In situ processing of electrically conducting graphene/SiC nanocomposites. J Eur Ceram Soc 2013;33(10):1665-74.

[27] Hummers WS, Offeman RE. Preparation of graphitic oxide. J Am Chem Soc 1958;80:1339.

[28] Lange FF. Powder processing science and technology for increased reliability. J Am Ceram Soc 1989;72:3-15.

[29] Garmendia N, Santacruz I, Moreno R, Obieta I. Slip casting of nanozirconia/MWCNT composites using a heterocoagulation process. J Eur Ceram Soc 2009;29:1939-45.

[30] Huh SH. Physics and applications of graphene-experiments. In: Sergey M, editor. Thermal reduction of graphene oxide. InTech; 2011. p. 73-90.

[31] Hannink RHJ, Kelly PM, Muddle BC. Transformation toughening in zirconia-containing ceramics. J Am Ceram Soc 2000;83:461-87.

[32] Evans AJ. Perspective on the development of high-toughness ceramics. J Am Ceram Soc 1990;73:187-206.

[33] Marshall DB, Ratto JJ, Lange FF. Enhanced fracture toughness in layered microcomposites of Ce-ZrO_2 and Al_2O_3. J Am Ceram Soc 1991;74: 2979-87.

[34] Lube T, Pascual J, Chalvet F, de Portu G. Effective fracture toughness in Al_2O_3-Al_2O_3/ZrO_2 laminates. J Eur Ceram Soc 2007;27:1449-53.

[35] Sglavo VM, Bertoldi M. Design and production of ceramic laminates with high mechanical resistance and reliability. Acta Mater 2006;54:4929-37.

[36] Bermejo R, Torres Y, Baudín C, Sánchez-Herencia AJ, Pascual J, Anglada M, Llanes L. Threshold strength evaluation on an Al_2O_3/ZrO_2 multilayered system. J Eur Ceram Soc 2007;27:1443-8.

[37] Requena J, Moreno R, Moya JS. Alumina and alumina zirconia multilayer composites obtained by slip casting. J Am Ceram Soc 1989;72:1511-3.

[38] Boch P, Chartier T, Huttepain M. Tape casting of Al_2O_3/ZrO_2 laminated composites. J Am Ceram Soc 1986;69(8):C191-2.

[39] Gurauskis J, Sánchez-Herencia AJ, Baudín C. Al_2O_3/Y-TZP and Y-TZP materials fabricated by stacking layers obtained by aqueous tape casting. J Eur Ceram Soc 2006;26:1489-96.

[40] Bermejo R, Baudín C, Moreno R, Sánchez-Herencia AJ, Llanes L. Processing optimisation and fracture behaviour of layered ceramic composites with highly compressive layers. Comp Sci Technol 2007;67:1930-38.

[41] Liu J, Yan H, Reece MJ, Jiang K. Toughening of zirconia/alumina composites by the addition of graphene platelets. J Eur Ceram Soc 2012;32:4185-93.

[42] Rincón A, Chinelatto ASA, Moreno R. Tape casting of alumina/zirconia suspensions containing graphene oxide. Submitted to J Eur Ceram Soc. http://dx.doi.org/10.1016/j.jeurceramsoc.2013.12.027

[43] Asmani M, Kermel C, Leriche A, Ourak M. Influence of porosity on Young's modulus and Poisson's ratio in alumina ceramics. J Eur Ceram Soc 2001;21:1081-86.

[44] Terrones M, Botello-Méndez A, Campos-Delgado J, López-Urías F, Vega-Cantú YI, Rodríguez-Macías FJ, Laura Elías A, Muñoz-Sandoval E, Cano-Márquez AG, Jean-Christophe CH. Graphene and graphite nanoribbons: Morphology, properties, synthesis, defects and applications. Nano Today 2010;5(4):351-72.

[45] Ferrari AC, Meyer JC, Scardaci V, Casiraghi C, Lazzeri M, Mauri F, Piscanec S, Jiang D, Novoselov KS, Roth S, Geim AK. Raman spectrum of graphene and graphene layers. Phys Review Lett 2006;97:187401.

[46] Park JS, Reina A, Saito R, Kong J, Dresselhaus G, Dresselhaus MS. G' band Raman spectra of single, double and triple layer graphene. Carbon 2009;47(5):1303-10.

[47] Puchegger S, Dose F, Loidl D, Kromp K, Janssen R, Brandhuber D, Hüsing N, Peterlik H. The dependence of the elastic moduli of reaction bonded alumina on porosity. J Eur Ceram Soc 2007;27(1):35-9.

[48] Porwal H, Tatarko P, Grasso S, Khaliq J, Dlouhý I, J. Reece M. Graphene reinforced alumina nano-composites. Carbon 2013;64:359-69.

[49] Rayón E, Moreno R, Alcazar C, Salvador MD, Manjón FJ, Jiménez-Piqué E, LLanes L. Enhanced hydrothermal resistance of Y-TZP ceramics through colloidal processing. J Am Ceram Soc 2013;96(4):1070-6.

[50] Trejo-Arroyo D, Zárate-Medina J, Alvarado-Orozco JM, Contreras-García ME, Boldrick MS, Muñoz-Saldaña J. Microstructure and mechanical properties of Al_2O_3-YSZ spherical polycrystalline composites. J Eur Ceram Soc 2013;33(10):1907-16.

Tables:

Table 1. Vickers hardness and mechanical properties obtained by nanoindentation technique of the A/AZ/AZGO sample. Nanoindentation results were averaged out in the range between 500 to 1000 nm in depth.

Layer	H_{IT} (GPa)	*Std. Dev*	E (GPa)	*Std. Dev.*	Er (GPa)	HV_{2kg}
A	27.0	*0.3*	409.8	*2.9*	395.8	2145
AZ	25.8	*0.4*	400.0	*3.7*	317.8	2020
AZGO	23.5	*0.3*	373.9	*3.1*	298.0	1856

Captions to figures:

Fig. 1. Schematic flow chart showing the preparation and configuration of the green multilayer compositions, including the following steps: (1) punching of green discs; (2) lamination of the layer to obtain symmetric 9-layers stacks at room conditions by pressing using water drops as gluing agent; 3) sintering of materials at 1400 ºC by SPS under vacuum and 80 MPa of pressure.

Fig. 2. Optical microscopy images of the three types of laminates sintered by SPS; A/AZ (a), AZ/AZGO (b), and A/AZ/AZGO (c), taken under dark field illumination. The brightest layers in (c) correspond to the AZGO composition while darkest ones are α-Al_2O_3.

Fig. 3. Optical microscopy picture showing the interfaces between the A, AZ and the AZGO layers in the sintered A/AZ/AZGO sample.

Fig. 4. FE-SEM images showing the fracture surfaces of the A layer (a), AZ layer (b), and AZGO layer (c). The arrow in (c) shows a possible few-layered graphene or graphite-detached film. This analysis was performed on the cross-section of fractured A/AZ/AZGO sample.

Fig. 5. FE-SEM image of a fracture surface of an AZGO layer in the A/AZ/AZGO composite, in which two thin films of graphene or few-layered graphite were captured.

Fig. 6. Raman spectra of Al_2O_3 (A) and Al_2O_3+5vol.% ZrO_2 (AZ) layers.

Fig. 7. Raman spectra of the D, G and 2D bands acquired on each layer of the A/AZ/AZGO sample. Analysis was performed on the cross-section of the polished and fractured sample except when the surface of the sintered disc was studied.

Fig. 8. Optical microscope image acquired on the cross-section of A/AZ/AZGO sample, revealing the Berkovich imprints performed at 1200 nm.

Fig. 9. Hardness and Young's modulus as a function of the indentation depth obtained by nanoindentation for each layer in the A/AZ/AZGO laminate.

Fig. 10. Elastic modulus (a) and nanohardness (b) profiles for indentations performed at 300 nm of depth on the entire width of the A/AZ/AZGO sample. Fig. 10c shows the array of Berkovich imprints distanced by 10 µm.

Figure
Click here to download high resolution image

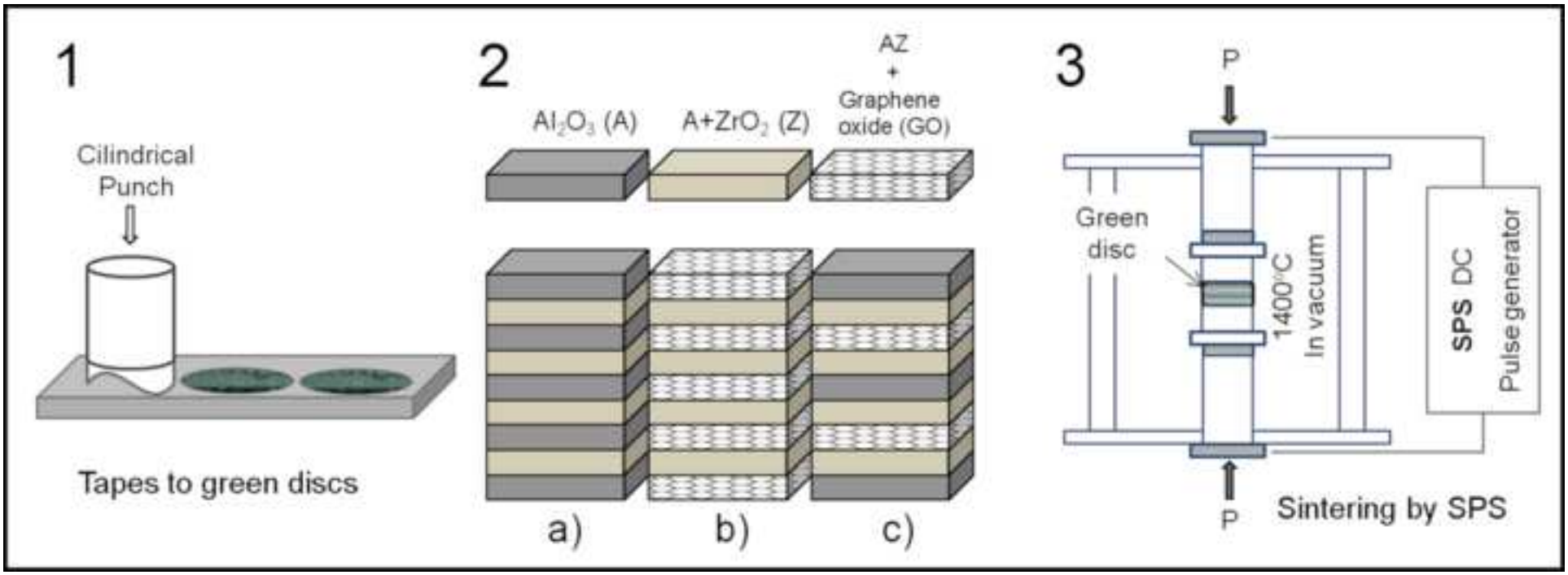

Figure
Click here to download high resolution image

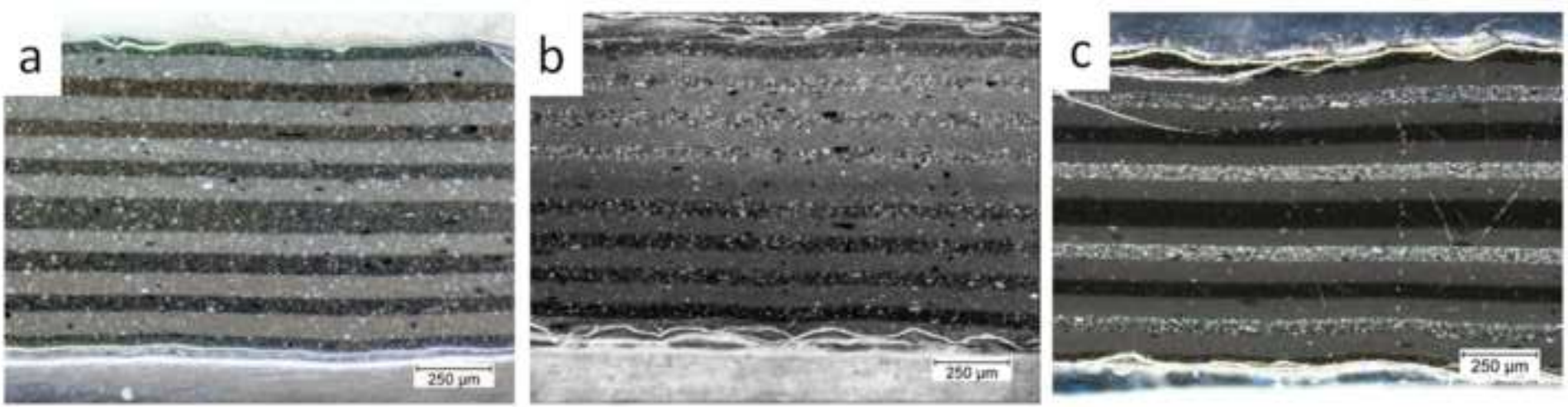

Figure

Click here to download high resolution image

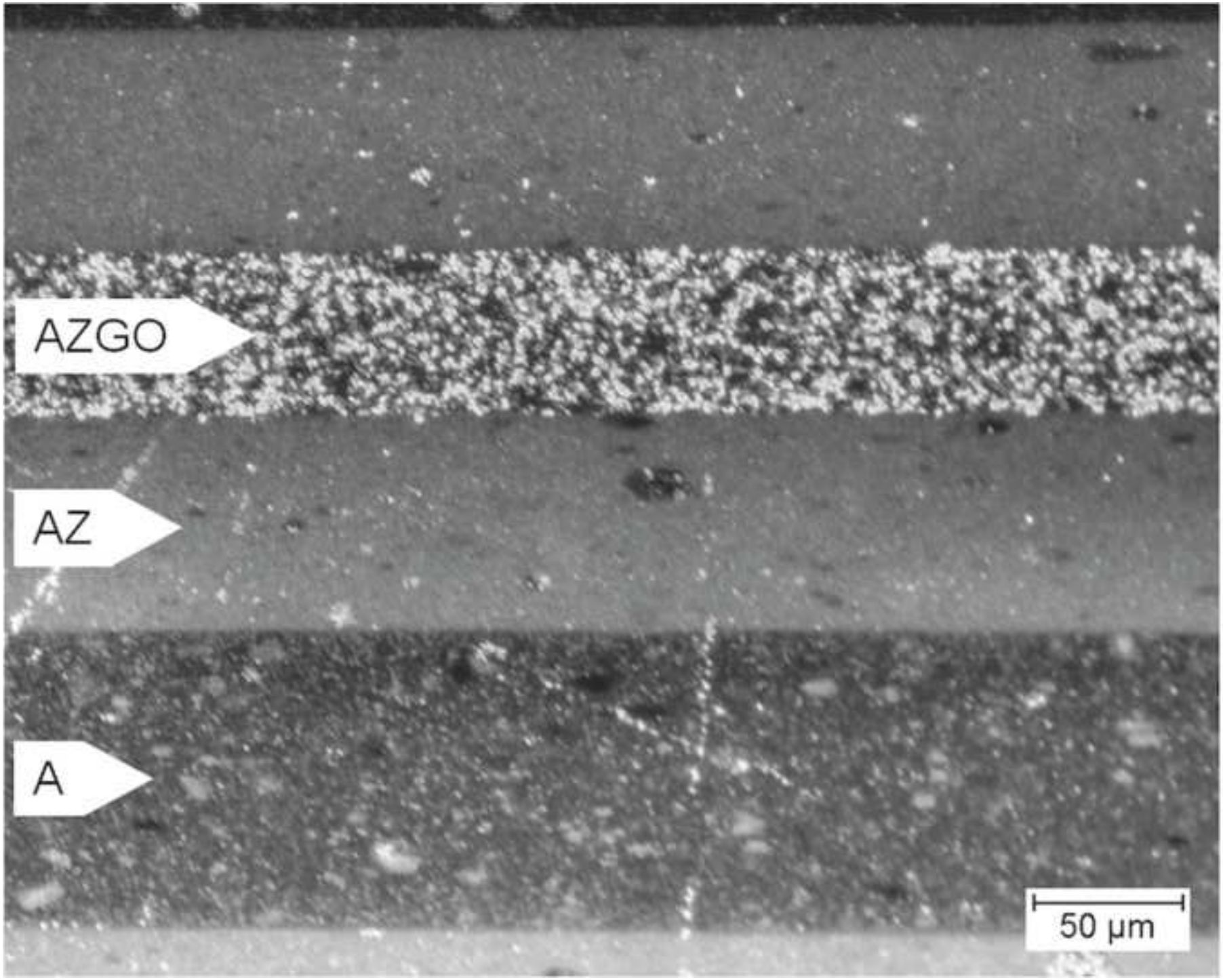

Figure

Click here to download high resolution image

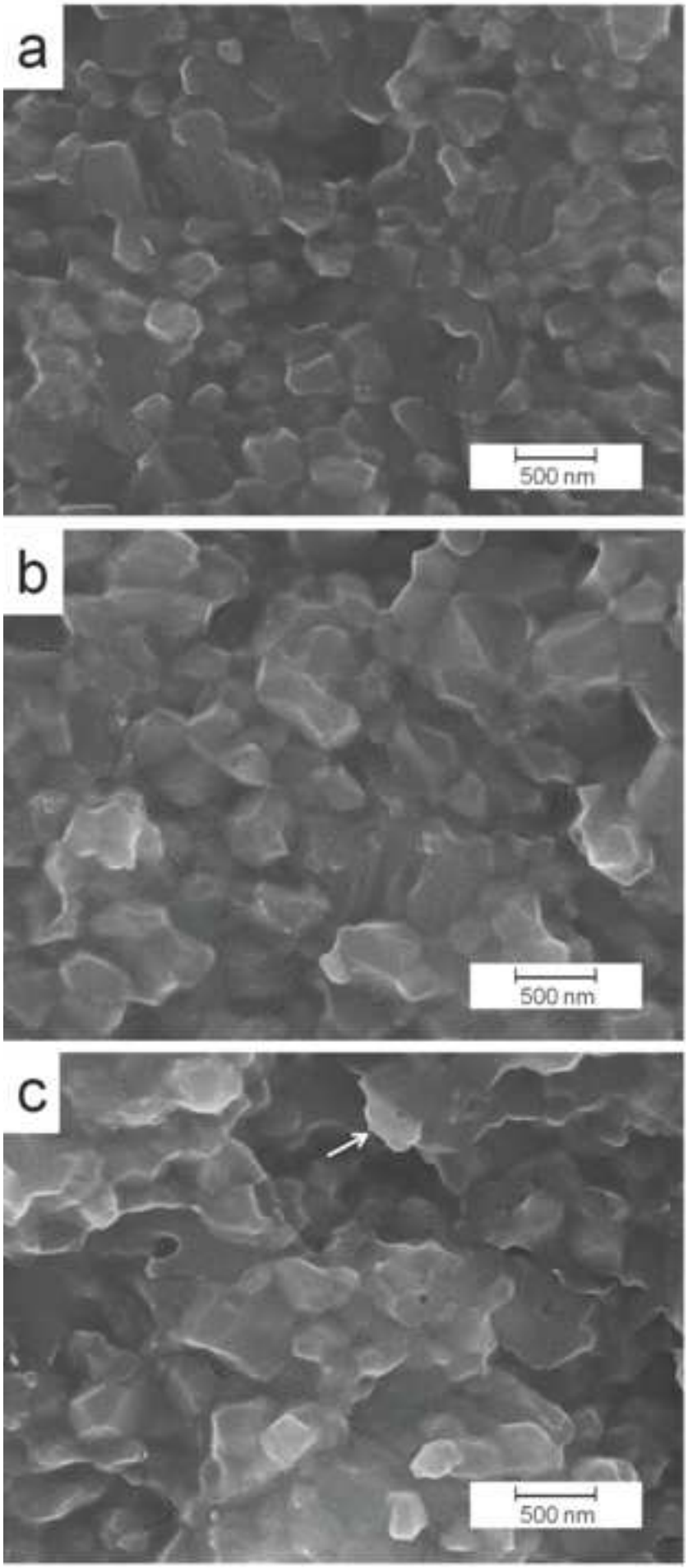

Figure

Click here to download high resolution image

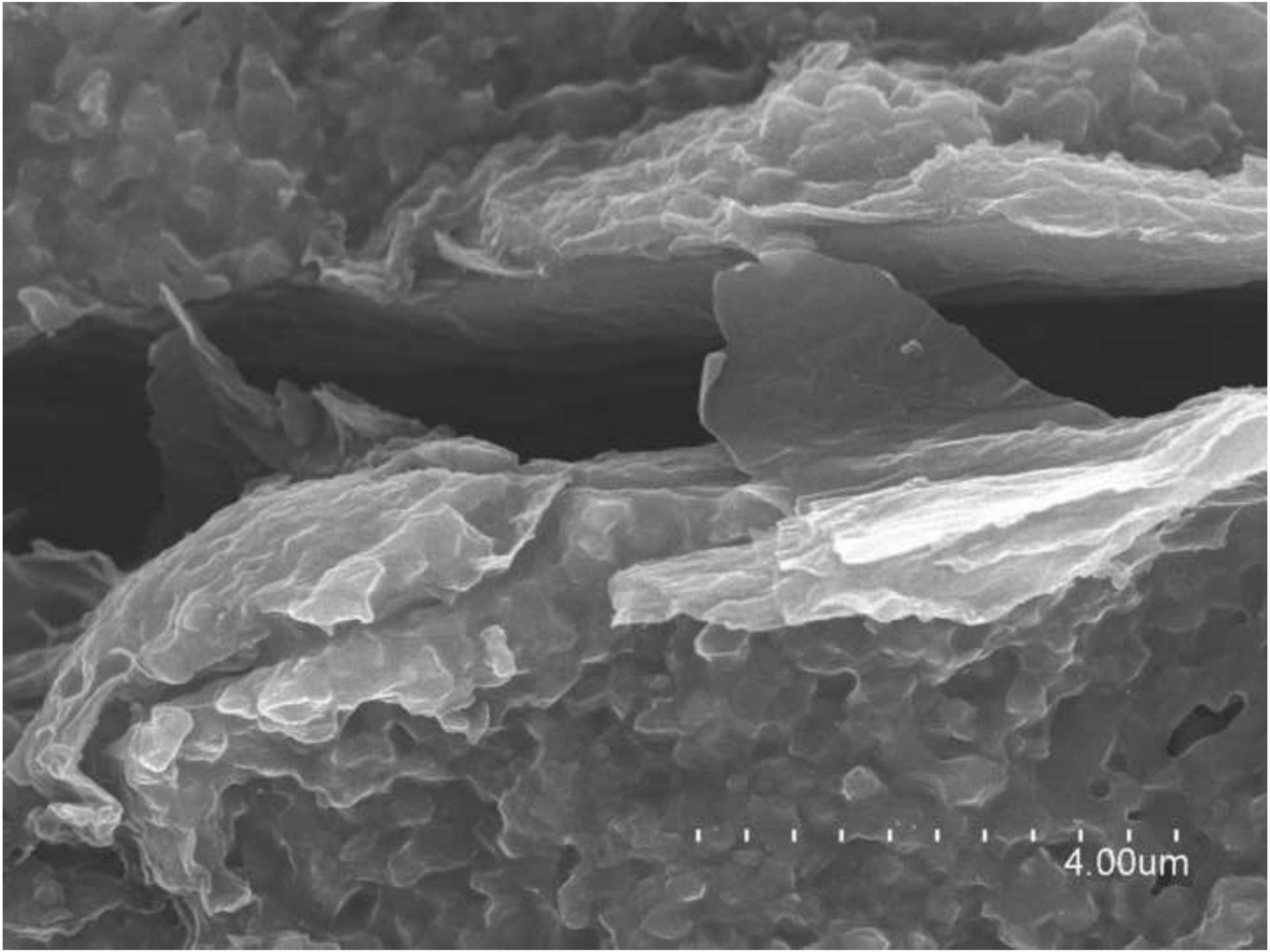

Figure
Click here to download high resolution image

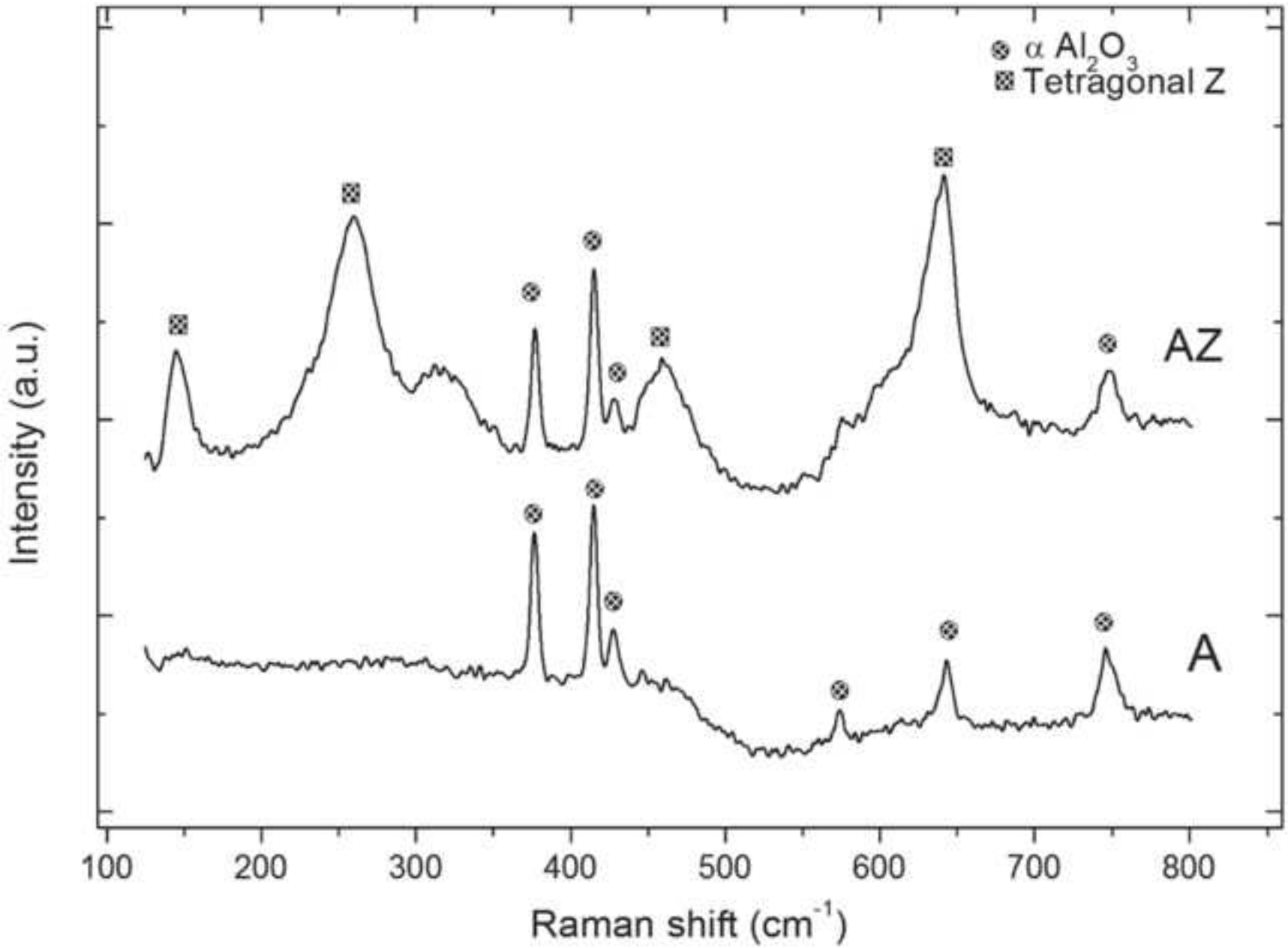

Figure
Click here to download high resolution image

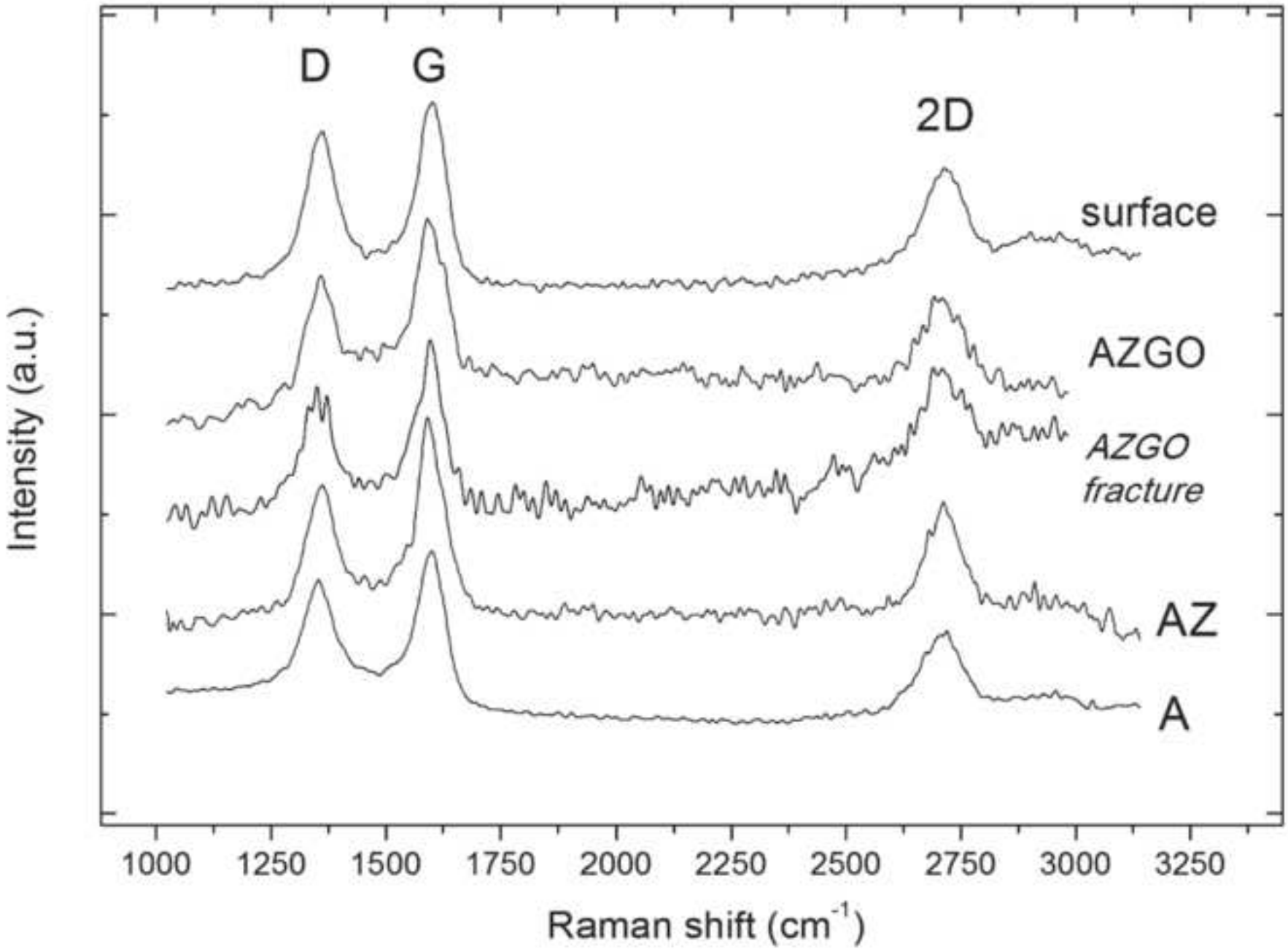

Figure

Click here to download high resolution image

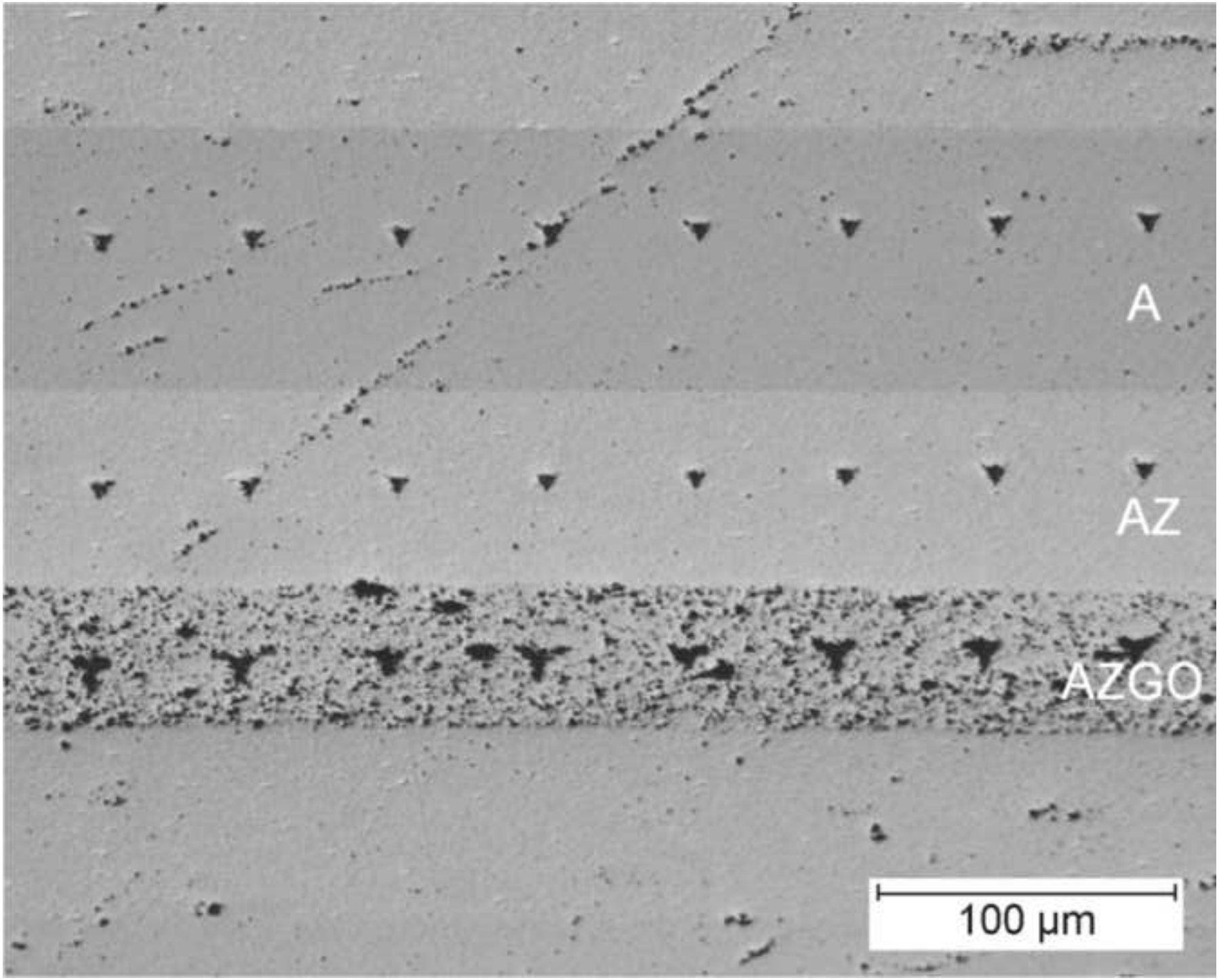

Figure
Click here to download high resolution image

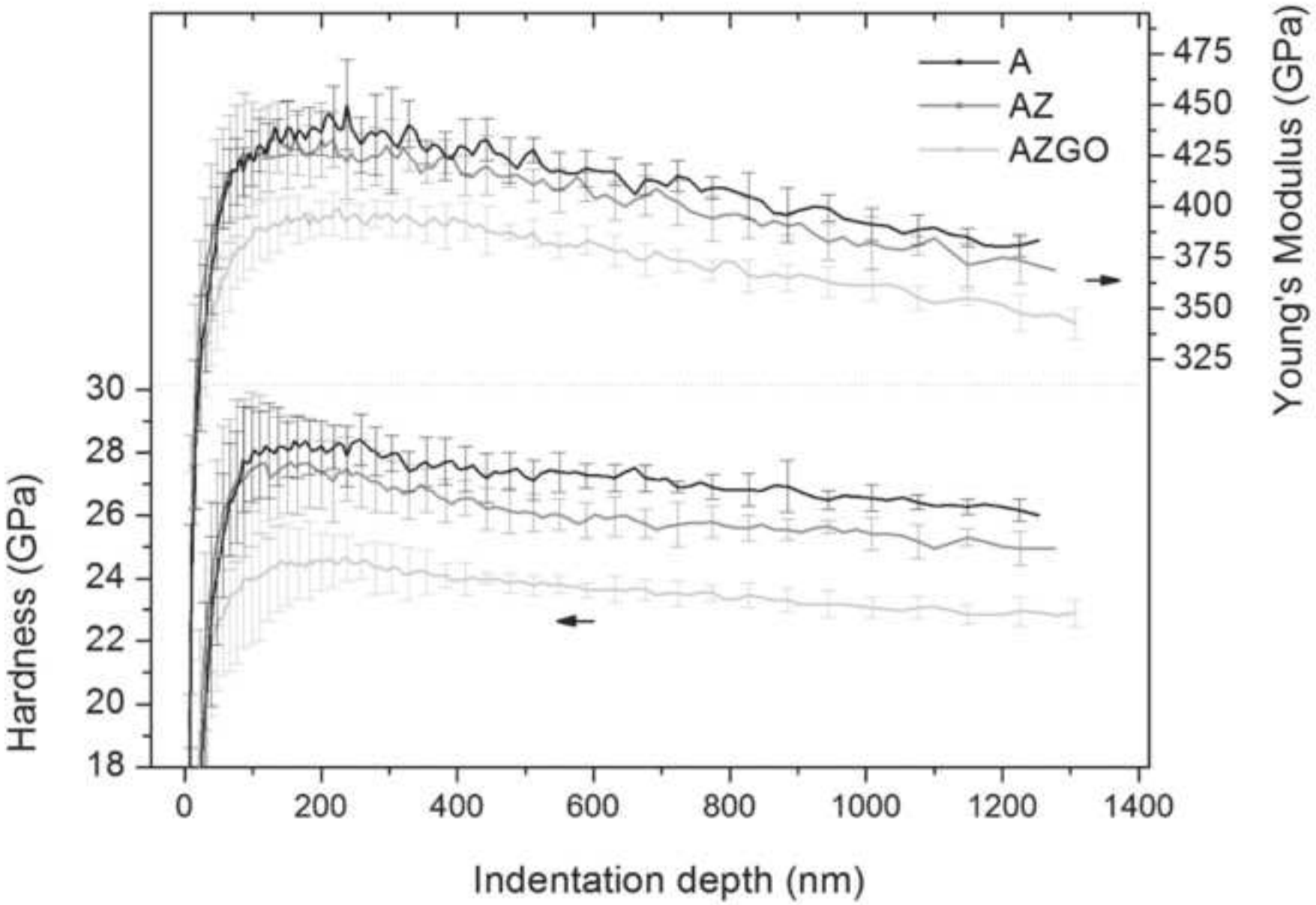

Figure

Click here to download high resolution image

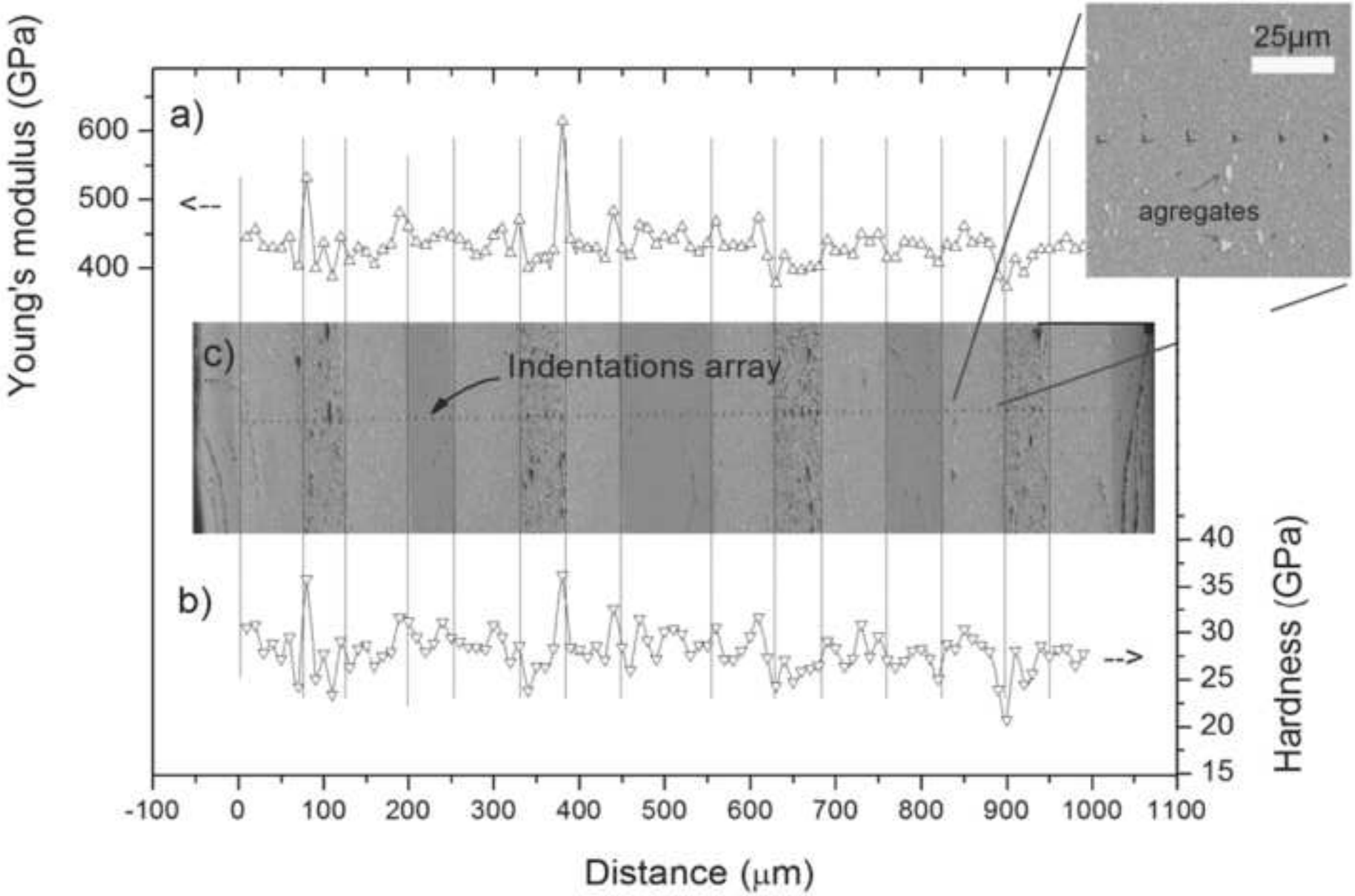

Captions to figures:

Fig. 1. Schematic flow chart showing the preparation and configuration of the green multilayer compositions, including the following steps: (1) punching of green discs; (2) lamination of the layer to obtain symmetric 9-layers stacks at room conditions by pressing using water drops as gluing agent; 3) sintering of materials at 1400 ºC by SPS under vacuum and 80 MPa of pressure.

Fig. 2. Optical microscopy images of the three types of laminates sintered by SPS; A/AZ (a), AZ/AZGO (b), and A/AZ/AZGO (c), taken under dark field illumination. The brightest layers in (c) correspond to the AZGO composition while darkest ones are α-Al_2O_3.

Fig. 3. Optical microscopy picture showing the interfaces between the A, AZ and the AZGO layers in the sintered A/AZ/AZGO sample.

Fig. 4. FE-SEM images showing the fracture surfaces of the A layer (a), AZ layer (b), and AZGO layer (c). The arrow in (c) shows a possible few-layered graphene or graphite-detached film. This analysis was performed on the cross-section of fractured A/AZ/AZGO sample.

Fig. 5. FE-SEM image of a fracture surface of an AZGO layer in the A/AZ/AZGO composite, in which two thin films of graphene or few-layered graphite were captured.

Fig. 6. Raman spectra of Al_2O_3 (A) and Al_2O_3+5vol.% ZrO_2 (AZ) layers.

Fig. 7. Raman spectra of the D, G and 2D bands acquired on each layer of the A/AZ/AZGO sample. Analysis was performed on the cross-section of the polished and fractured sample except when the surface of the sintered disc was studied.

Fig. 8. Optical microscope image acquired on the cross-section of A/AZ/AZGO sample, revealing the Berkovich imprints performed at 1200 nm.

Fig. 9. Hardness and Young's modulus as a function of the indentation depth obtained by nanoindentation for each layer in the A/AZ/AZGO laminate.

Fig. 10. Elastic modulus (a) and nanohardness (b) profiles for indentations performed at 300 nm of depth on the entire width of the A/AZ/AZGO sample. Fig. 10c shows the array of Berkovich imprints distanced by 10 µm.